The Astronomical Journal, 145:155 (15pp), 2013 June doi:10.1088/0004-6256/145/6/155

VERY LOW MASS STELLAR AND SUBSTELLAR COMPANIONS TO SOLAR-LIKE STARS FROM MARVELS. V. A LOW ECCENTRICITY BROWN DWARF FROM THE DRIEST PART OF THE DESERT, MARVELS-6b

Nathan De Lee[1,2,3], Jian Ge[3], Justin R. Crepp[4], Jason Eastman[5,6,7], Massimiliano Esposito[8,9], Bruno Femenía[8,9], Scott W. Fleming[3,10,11,12], B. Scott Gaudi[5], Luan Ghezzi[13,14], Jonay I. González Hernández[8,9], Brian L. Lee[3,15], Keivan G. Stassun[1,2], John P. Wisniewski[16], W. Michael Wood-Vasey[17], Eric Agol[15], Carlos Allende Prieto[8,9], Rory Barnes[15], Dmitry Bizyaev[18], Phillip Cargile[1], Liang Chang[3], Luiz N. Da Costa[13,14], G. F. Porto De Mello[14,19], Leticia D. Ferreira[14,19], Bruce Gary[1], Leslie Hebb[1,15], Jon Holtzman[20], Jian Liu[3], Bo Ma[3], Claude E. Mack III[1], Suvrath Mahadevan[10,11], Marcio A. G. Maia[13,14], Duy Cuong Nguyen[3,21], Audrey Oravetz[18], Daniel J. Oravetz[18], Martin Paegert[1], Kaike Pan[18], Joshua Pepper[1], Elena Malanushenko[18], Viktor Malanushenko[18], Rafael Rebolo[8,9,22], Basilio X. Santiago[14,23], Donald P. Schneider[10,11], Alaina C. Shelden Bradley[18], Xiaoke Wan[3], Ji Wang[3], and Bo Zhao[3]

[1] Department of Physics and Astronomy, Vanderbilt University, Nashville, TN 37235, USA; nathan.delee@vanderbilt.edu
[2] Department of Physics, Fisk University, Nashville, TN, USA
[3] Department of Astronomy, University of Florida, 211 Bryant Space Science Center, Gainesville, FL 32611-2055, USA
[4] Department of Physics, University of Notre Dame, 225 Nieuwland Science Hall, Notre Dame, IN 46556, USA
[5] Department of Astronomy, The Ohio State University, 140 West 18th Avenue, Columbus, OH 43210, USA
[6] Las Cumbres Observatory Global Telescope Network, 6740 Cortona Drive, Suite 102, Santa Barbara, CA 93117, USA
[7] Department of Physics Broida Hall, University of California, Santa Barbara, CA 93106, USA
[8] Instituto de Astrofísica de Canarias (IAC), E-38205 La Laguna, Tenerife, Spain
[9] Departamento de Astrofísica, Universidad de La Laguna, E-38206 La Laguna, Tenerife, Spain
[10] Department of Astronomy and Astrophysics, The Pennsylvania State University, 525 Davey Laboratory, University Park, PA 16802, USA
[11] Center for Exoplanets and Habitable Worlds, Pennsylvania State University, University Park, PA 16802, USA
[12] Space Telescope Science Institute, 3700 San Martin Drive, Baltimore, MD 21218, USA
[13] Observatório Nacional, Rua Gal. José Cristino 77, Rio de Janeiro, RJ 20921-400, Brazil
[14] Laboratório Interinstitucional de e-Astronomia - LIneA, Rua Gal. José Cristino 77, Rio de Janeiro, RJ 20921- 400, Brazil
[15] Astronomy Department, University of Washington, Box 351580, Seattle, WA 98195, USA
[16] H L Dodge Department of Physics and Astronomy, University of Oklahoma, 440 W Brooks St Norman, OK 73019, USA
[17] Pittsburgh Particle physics, Astrophysics, and Cosmology Center (PITT PACC), Department of Physics and Astronomy, University of Pittsburgh, Pittsburgh, PA 15260, USA
[18] Apache Point Observatory, P.O. Box 59, Sunspot, NM 88349-0059, USA
[19] Universidade Federal do Rio de Janeiro, Observatório do Valongo, Ladeira do Pedro Antonio 43, 20080-090 Rio de Janeiro, Brazil
[20] Department of Astronomy, New Mexico State University, Box 30001, Las Cruces, NM 880033, USA
[21] Department of Physics and Astronomy, University of Rochester, Rochester, NY 14627-0171, USA
[22] Consejo Superior de Investigaciones Científicas, Calle Serrano, 117, 28006 Madrid, Spain
[23] Instituto de Fisica, UFRGS, Porto Alegre, RS 91501-970, Brazil
Received 2013 February 1; accepted 2013 April 8; published 2013 May 6

ABSTRACT

We describe the discovery of a likely brown dwarf (BD) companion with a minimum mass of 31.7 ± 2.0 $M_{\rm Jup}$ to GSC 03546-01452 from the MARVELS radial velocity survey, which we designate as MARVELS-6b. For reasonable priors, our analysis gives a probability of 72% that MARVELS-6b has a mass below the hydrogen-burning limit of 0.072 $M_{\odot}$, and thus it is a high-confidence BD companion. It has a moderately long orbital period of $47.8929^{+0.0063}_{-0.0062}$ days with a low eccentricity of $0.1442^{+0.0078}_{-0.0073}$, and a semi-amplitude of 1644^{+12}_{-13} m s^{-1}. Moderate resolution spectroscopy of the host star has determined the following parameters: $T_{\rm eff} = 5598 \pm 63$, $\log g = 4.44 \pm 0.17$, and [Fe/H] = +0.40 ± 0.09. Based upon these measurements, GSC 03546-01452 has a probable mass and radius of $M_* = 1.11 \pm 0.11\ M_{\odot}$ and $R_* = 1.06 \pm 0.23\ R_{\odot}$ with an age consistent with less than ∼6 Gyr at a distance of 219 ± 21 pc from the Sun. Although MARVELS-6b is not observed to transit, we cannot definitively rule out a transiting configuration based on our observations. There is a visual companion detected with Lucky Imaging at 7.″7 from the host star, but our analysis shows that it is not bound to this system. The minimum mass of MARVELS-6b exists at the minimum of the mass functions for both stars and planets, making this a rare object even compared to other BDs. It also exists in an underdense region in both period/eccentricity and metallicity/eccentricity space.

Key words: brown dwarfs – stars: individual (GSC 03546-01452)

Online-only material: color figures, Supplemental data (FITS) file (tar.gz)

1. INTRODUCTION

Radial velocity (RV) surveys have provided a wealth of exoplanet discoveries around sun-like stars in recent years (California Planet Survey, Howard et al. 2010; Lick-Carnegie Exoplanet Survey, Haghighipour et al. 2010; CORALIE survey, Udry et al. 2000; and the HARPS survey, Mayor et al. 2003 to name a few), but they have not found a correspondingly large number of brown dwarf (BD) companions (Reid & Metchev 2008). BD companions lie on the mass spectrum between planets and stars and are defined as being between 13 $M_{\rm Jup}$ and 75.5 $M_{\rm Jup}$ (based on the deuterium and hydrogen fusion limits; Chabrier et al. 2000; Spiegel et al. 2011). The lack of BDs within 3 AU of their host star was first recognized in

Marcy & Butler (2000), and is known as the BD "desert." This result is unlikely to be due to observational bias because the RV semiamplitudes of BD are many hundreds to a few thousand meters per second, which is easily detectable by these surveys (Patel et al. 2007). Thus the lack of BD at close to moderate distances from their respective host stars points to an explanation based in BD formation mechanisms.

Although the formation of low-mass companions (planets through low mass stars) to sun-like stars is still an area of active research, in overview there are two main mechanisms: planets form from a protoplanetary disks and stellar companions (in a similar range of separations) from molecular cloud fragmentation. Given the mass range of BD companions, they could form through either mechanism (or both). Understanding the origin of the BD desert can put major constraints on the upper mass limit for companion formation in protoplanetary disks, and a lower mass limit on formation via fragmentation.

Recent efforts to quantify the frequency of companions as a function of mass in the BD desert have found that the overall frequency of BD companions at close to moderate distances from their host star ($\leqslant$10 AU) is less than $<$1% (Grether & Lineweaver 2006), and more recently 0.6% (Sahlmann et al. 2011). This value is low compared to $\sim$7% for planetary companions (Udry & Santos 2007) and $\sim$13% for stellar companions in a similar range of separations (Duquennoy & Mayor 1991; Halbwachs et al. 2003). Grether & Lineweaver (2006) went a step further and defined the driest part of the desert to be where there was a minimum in the number of companions per unit interval in log mass; they found this position to be at a companion mass of 31^{+25}_{-18} $M_{\rm Jup}$.

This is the fifth paper in this series looking at low-mass companions to sun-like stars from the third generation of the Sloan Digital Sky Survey (SDSS-III; Eisenstein et al. 2011) Multi-Object APO Radial Velocity Exoplanet Large-Area Survey (MARVELS; Ge et al. 2008, 2009; Ge & Eisenstein 2009). The primary goal of this series is to provide a detailed set of well-characterized companions with minimum masses and separations in or near the BD desert, which can be used by future meta-analyzes. Ultimately, this is the sort of groundwork that must be done in order to understand the extent and aridity of the BD desert.

The MARVELS survey measured radial velocities of 3,300 unique FGK type stars. MARVELS is a large survey looking for RV companions around bright stars ($7.6 \leqslant V \leqslant 12$) with periods below 2 yr with well characterized biases; see Lee et al. (2011) for a description of the survey design. Other papers in this series (Fleming et al. 2010, 2012; Wisniewski et al. 2012; Ma et al. 2013, Mack et al. 2013; Jiang et al. 2013) have helped fill in our understanding of the BD desert, and provided warnings to some of the pitfalls inherent in these analyzes.

We will discuss observations of the star GSC 03546-01452, which has a companion with a period of $\sim$47 days and with a minimum mass of 31.7 ± 2.0 $M_{\rm Jup}$ placing it near the most "arid" region of the BD desert. In Section 2, we discuss the photometric and spectroscopic observations and basic data processing. In Section 3, we discuss the analysis of this data. Section 4 contains a discussion of the results and places MARVELS-6b within the larger context. Section 5 summarizes our results.

2. OBSERVATIONS AND DATA REDUCTION

The initial detection and orbital characterization of MARVELS-6b came from the MARVELS Survey RV data. Once it became a strong candidate, further RV, photometric, time-series photometric, and spectroscopic data were taken to confirm this candidate. Each of these data sets will be discussed below.

2.1. Initial Identification of MARVELS Candidates

2.1.1. Survey Summary

MARVELS is a multi-epoch radial velocity survey designed to detect radial velocity companions around FGK type stars in a magnitude range of ($7.6 \leqslant V \leqslant 12$). It uses a dispersed fixed-delay interferometer (DFDI; Ge et al. 2009) on the SDSS 2.5 m telescope (Gunn et al. 2006). The DFDI method was introduced for use in a multi-object RV survey by Ge (2002). A single object version of a DFDI instrument was successfully used to detect a hot Jupiter around HD 102195 (Ge et al. 2006). The DFDI instrument principle was described by Ge (2002), Ge et al. (2002), Erskine (2003), van Eyken et al. (2010), and Wang et al. (2011). The MARVELS interferometer delay calibrations were described in Wang et al. (2012a, 2012b).

Each MARVELS observation consists of 60 stars spread across 120 spectra (2 spectra for each star). The MARVELS survey started in 2008 October and ran through 2012 July. It was divided up into two observing sets: year 1–2 fields which were observed from 2008 October till 2011 January and year 3–4 fields which were observed from 2011 January till 2012 July.

The year 1–2 data set consisted of 43 unique fields (11 of which are in the *Kepler*; Borucki et al. 2010). The year 3–4 field set contained 13 fields (with 1 field overlapping the year 1–2 field set.) This leads to a total of 3,300 unique stars with $>$18 epochs.

2.1.2. Radial Velocity Analysis Software

The large number of RV targets required the development of a software package to easily display and characterize the radial velocity curves from the MARVELS survey. One of the primary tools used in this process is an IDL-based Keplerian model fitter known as MPRVFIT.[24] MPRVFIT starts with the input of RV data in the form of Julian date, RV, and RV error (the Julian date and RVs can be of any type that is appropriate to the analysis). In the case of MARVELS, the data from the two beams have been combined as described in Fleming et al. (2010). The software then applies a modified version of the Lomb–Scargle periodogram (Lomb 1976; Scargle 1982) described in Cumming (2004). False alarm probabilities were assigned to the highest peaks using the formulation of Baluev (2008). Once a number of high probability peaks are identified, the frequency space between the peak and the next nearest frequency point in the periodogram is sub-divided into 10 frequency steps (on both sides of the peak). A Keplerian model is then fit to those frequencies using MPFIT (Markwardt 2009). MPFIT is a Levenberg–Marquardt non-linear least squares fitter implemented in IDL. The χ^2 statistic is determined for each fit, and the best chi-squared fit of the grid is retained. Finally, the best fit models are plotted with the data points for easy reference. For the MARVELS survey, the two best fits for each target were displayed, and the candidates were chosen based on the folded and unfolded radial velocity curves, as well as the significance of the periodogram. An example of this periodogram for GSC 03546-01452 can be found in Figure 1.

[24] http://www.vanderbilt.edu/AnS/physics/vida/mprvfit.htm

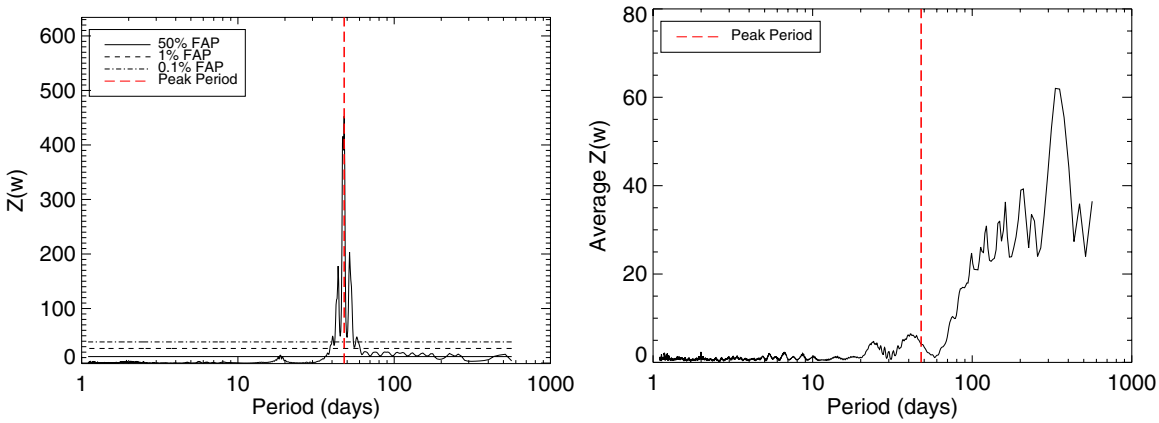

Figure 1. Left: the original detection Lomb–Scargle periodogram for GSC 03546-01452 based on the MARVELS data. The two RV points with the lowest spectrum flux were removed for this initial periodogram (as marked in Table 1). The peak in the periodogram (marked by the red dashed line) is quite significant and is at 47.842 days, close to the final adopted value of 47.893 days for the combined MARVELS and TNG/SARG data. Right: a combined periodogram for all 60 stars on the MARVELS plate. The highest power point in each frequency bin was removed, and the remaining were averaged. The red dashed line shows the peak period from the periodogram on the left. There is no obvious systematic peak on the plate periodogram at the peak period of the GSC 03546-01452 periodogram.

(A color version of this figure is available in the online journal.)

2.2. Radial Velocities

2.2.1. SDSS-II MARVELS Radial Velocities

Differential RV observations of GSC 03546-01452 were acquired during the first two years of the SDSS-III MARVELS survey. A total of 22 observations were obtained over the course of 565 days. As discussed in Section 2.1.1, the MARVELS survey uses the DFDI technique which introduces an interferometer into the light path. As a result, each 50 minute observation includes two fringed spectra, or beams, one from each arm of the interferometer. Each spectrum spans a wavelength range roughly 500–570 nm with a $R \sim 12{,}000$ resolution. Each beam is processed individually through the MARVELS pipeline following the methods described in Lee et al. (2011).

The formal errors derived from the MARVELS pipeline are known to be underestimates of the true error. This systematic underestimate can be partially corrected for by using the fact that 60 stars (120 beams) are taken in each observation. Following the method outlined in Fleming et al. (2010), it is expected that most stars in an observation plate are radial velocity stable, so the median rms is a reasonable estimate of the systematic errors. A quality factor (QF) is derived for each beam, which is the ratio of the radial velocity rms to the median formal error bar, and the median QF is found for the plate. The formal errors are multiplied by this QF (2.334 for GSC 03546-01452), resulting in the error bars used for the analysis of these observations. During the RV analysis, discussed in Section 3.2, it was determined that these scaled error bars were themselves overestimated, leading to a reduction of a factor of 0.5794. The final differential RV measurements and final scaled error bars (approximately 40% larger than the formal uncertainties) for GSC 03546-01452 are presented in Table 1.

2.2.2. TNG Differential Radial Velocities

Once GSC 03546-01452 was determined to be a candidate for additional investigation, spectroscopic observations were conducted with the Spettrografo Alta Risoluzione Galileo (SARG; Gratton et al. 2001) on the 3.6 m Telescopio Nazionale Galileo (TNG) located at Roque de Los Muchachos Observatory (ORM). All the spectra were acquired using the same instrumental configuration: a slit with a sky-projected width of 0.″8 achieving a resolving power of $R = 57000$; a yellow cross-dispersing grism providing the wavelength range $462 < \lambda < 792$ nm.

A total of 15 spectra were taken (11 with and 4 without the iodine cell inserted in the light path). One spectrum with the

Table 1
Summary of Radial Velocity Data

BJD (days)	RV (m s^{-1})	RV Err (m s^{-1})	Source ...
2454956.915966	2039.20	72.10	MARVELS[a]
2454957.946510	2150.89	43.11	MARVELS
2454958.912457	2206.71	39.27	MARVELS
2454959.927110	2291.25	36.06	MARVELS
2454962.924107	2568.84	36.54	MARVELS
2454963.890111	2559.01	48.00	MARVELS
2454964.918085	2529.69	39.97	MARVELS
2454965.910038	2579.81	43.36	MARVELS
2454984.835892	−797.93	41.72	MARVELS
2454986.892198	−736.07	43.95	MARVELS
2454988.905306	−444.95	40.44	MARVELS
2454990.799823	−154.83	64.34	MARVELS
2454993.804470	255.99	43.11	MARVELS
2454994.793741	543.09	49.32	MARVELS
2454995.898027	594.44	43.11	MARVELS
2455014.802962	2438.46	51.41	MARVELS
2455020.845356	1639.58	39.45	MARVELS
2455021.851131	1381.28	50.68	MARVELS
2455023.835931	792.32	53.52	MARVELS
2455024.788660	463.02	51.78	MARVELS
2455484.614289	2165.40	59.70	MARVELS
2455436.578251	1901.69	24.22	TNG/SARG
2455460.467627	−841.33	4.49	TNG/SARG
2455460.489293	−833.73	4.44	TNG/SARG
2455460.511619	−836.81	4.76	TNG/SARG
2455521.551045	722.14	88.25	MARVELS[b]
2455725.687910	1962.38	6.86	TNG/SARG
2455760.505697	66.39	9.99	TNG/SARG
2455760.694598	98.71	5.87	TNG/SARG
2455791.532669	122.53	5.96	TNG/SARG
2455791.583907	82.56	5.52	TNG/SARG
2455844.434368	−834.69	5.08	TNG/SARG

Notes.
[a] Second lowest flux spectrum.
[b] The lowest flux spectrum.

Table 2
SARG/TNG Absolute Radial Velocities

BJD days	RV (km s^{-1})	RV Err (km s^{-1})
2455436.550647	−12.63	0.13
2455436.578251	−12.73	0.13
2455460.467627	−15.43	0.13
2455460.489293	−15.35	0.13
2455460.511619	−15.41	0.13
2455698.630462	−15.28	0.13
2455698.654826	−15.30	0.13
2455725.687910	−12.48	0.13
2455760.505697	−14.39	0.13
2455760.694598	−14.32	0.13
2455791.532669	−14.36	0.13
2455791.583907	−14.22	0.13
2455791.610041	−14.43	0.13
2455791.635364	−14.52	0.13
2455844.434368	−15.48	0.13

iodine cell proved to have too low signal-to-noise ratio (S/N), leaving only 10 spectra suitable for differential velocity measurements. The spectra were processed using the standard IRAF[25] Echelle reduction packages. The S/N per resolution element at 550 nm ranges from 50 to 130. The spectra without I2 lines served as a reference for measuring the relative radial velocities of the 10 spectra with superimposed I2 absorption lines. The technique adopted to derive RV values is described in Marcy & Butler (1992). For details on how the technique was implemented on SARG spectra, see Fleming et al. (2012). As is the case with the MARVELS RV data, the formal uncertainties for the TNG/SARG data were overestimated, and so the error bars were thus reduced by a factor of 0.2224. The final differential RV and reduced error bars are listed in Table 1.

2.2.3. TNG Absolute Radial Velocities

All 15 spectra taken with the TNG/SARG instrument were used to calculate absolute RVs. The stellar spectra were cross-correlated with a high resolution solar spectrum.[26] The cross-correlation was done using the SARG red CCD spectrum with a wavelength coverage of 6200–8000 Å. Due to the non-simultaneity of the ThAr wavelength calibration exposures, it is possible that the slit illumination varied between the science spectra and the calibration spectra, which could result in the RV measurement being affected by systematic errors. To partially mitigate this error source, we calculated the cross-correlation function of the telluric lines (Griffin & Griffin 1973) around 6900 Å with a numerical mask. This exercise results in an RV correction of a few hundred m s^{-1}. This correction plus the barycentric correction were applied to the radial velocities and the resulting values are shown in Table 2.

To validate this method, observations of the RV standard star HD3765 were used. The standard was observed at 8 epochs with a mean result of −63,155 m s^{-1} ± 128 m s^{-1}. This result is within a 1σ agreement with the mean 34 observations taken from the ELODIE archive of −63,286 ± 49 m s^{-1}. For these observations, the systematics caused by the non-simultaneity of the ThAr wavelength calibration is the dominant error source, so we adopt ±128 m s^{-1} for the error in these measurements.

[25] IRAF is distributed by the National Optical Astronomy Observatory, which is operated by the Association of Universities for Research in Astronomy, Inc., under cooperative agreement with the National Science Foundation.
[26] http://bass2000.obspm.fr/solar_spect.php

2.3. High-resolution Spectrum for Stellar Classification

Two $R \sim 31{,}500$ optical (∼3600–10,000 Å) spectra of GSC 03546-01452 were obtained on UT 2010 June 20 with the Apache Point Observatory 3.5 m telescope and ARC Echelle Spectrograph (ARCES; Wang et al. 2003) to enable accurate characterization of stellar fundamental parameters ($T_{\rm eff}$, log g, and [Fe/H]). The two spectra were obtained using the default 1.6 × 3.2 arcsec slit and an exposure time of 1200 s for each spectra (for a combined exposure time of 2400 s). A ThAr lamp exposure was obtained after each of these integrations to facilitate accurate wavelength calibration. The data were processed using standard IRAF techniques. Following heliocentric velocity corrections, each order was continuum-normalized, and the resultant continuum-normalized data from each observation were averaged. The final spectrum yielded an S/N of approximately 110 per resolution element in the region around 6000 Å.

2.4. Photometry

2.4.1. HAO Absolute Photometry

We used the Hereford Arizona Observatory (HAO), a private facility in southern Arizona (observatory code G95 in the IAU Minor Planet Center), to measure multi-band, absolute photometry of GSC 03546-01452. HAO employs a 14 inch Meade Schmidt-Cassegrain (model LX200GPS) telescope, fork-mounted on an equatorial wedge located in a dome. The telescope's CCD is an SBIG ST-10XME with a KAF-3200ME detector. A 10-position filter wheel accommodates SDSS and Johnson/Cousins filter sets. GSC 03546-01452 and standard stars were observed with Johnson B and SDSS u', g', r', i' filters (Fukugita et al. 1996). For the Johnson–Kron–Cousins bands, standard stars are taken from the list published by Landolt & Uomoto (2007) and Landolt (2009). For the SDSS bands, standard stars are taken from the list published by Smith et al. (2002). Observations were conducted on three dates: 2010 April 24 and 25 and on 2010 May 7. Between 23 and 75 standard stars (Landolt and SDSS) were used to establish the transformations to the standard photometric systems.

2.4.2. Allegheny Lightcurve

We obtained 44 nights of observations of GSC 03546-01452 with the 16 inch Keeler RCX-400 Meade telescope at the Allegheny Observatory, University of Pittsburgh. The observations span 18 months from 2010 May through 2011 November and were all made through a Cousins R filter onto an SBIG KAF-6303E/LE 2048 × 3072 pixel CCD with a pixel scale of 0.″57 pixel^{-1} for a total FoV of 19.′5 by 29.′2. Exposure times ranged from 30 to 150 s depending on conditions, with a median exposure time of 75 s.

Standard bias and dark subtraction and flatfield calibrations were preformed on the raw data, and the images were astrometrically calibrated to the Two Micron All Sky Survey (2MASS) Point-Source Catalog (Skrutskie et al. 2006). Typical seeing conditions were between 3″and 4″ with a median seeing of 3.″5. Photometry was accomplished using a 10-pixel (5.″7) circular aperture and subtracting the estimated sky flux based on a 15–20 pixel (8.″6–11.″4) radius sky annulus. Typical 1σ uncertainties were 5 mmag. Relative photometry was calculated relative to the average counts from two reference stars in the image with J2000 coordinates: (1) 19:11:34.733 +48:34:54.77; and (2) 19:11:56.335 +48:22:55.38.

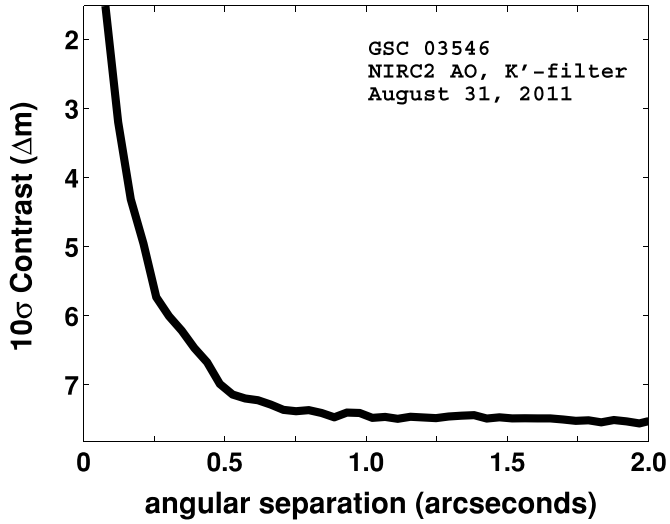

Figure 2. Contrast generated by NIRC2 AO observations of GSC 03546-01452. Off-axis sources with relative brightness $\Delta K' = 7$ are ruled out at 10σ for angular separations beyond $\approx 0\farcs5$.

2.4.3. SuperWASP Lightcurve

The SuperWASP survey (Pollacco et al. 2006) is a wide-angle transiting planet survey that monitors the brightness of millions of stars. The survey uses a visual broad band filter that covers the wavelength range from 400–700 nm. For details on reduction techniques and survey design please consult Pollacco et al. (2006). The SuperWASP photometry for GSC 03546-01452 consists of 8823 points spanning just over 4 yr from 2004 May to 2008 August.

2.5. High Spatial Resolution Imaging

Two high spatial resolution imaging campaigns of GSC 03546-01452 were undertaken in order to help rule out false positives and to look for hierarchical structure. In particular, these observations were conducted to search for visual companions at large separations that could influence our spectroscopic results, or that might be bound tertiary companions to GSC 03546-01452. The adaptive optics imaging and lucky imaging runs are complimentary with the adaptive optics focusing near the star and lucky imaging covering out to larger distances from the star.

2.5.1. Adaptive Optics Imaging

We also acquired adaptive optics (AO) observations of GSC 03546-01452 to assess its multiplicity at wide separations. Images were obtained on UT 2011 August 31 using NIRC2 (PI: Keith Matthews) at the 10 m Keck II telescope (Wizinowich et al. 2000). GSC 03546-01452 ($V = 11.7$) is sufficiently bright to serve as its own natural guide star. Our observations consist of 9 dithered images (10 coadds per frame, 0.5 s per coadd) taken with the K' filter ($\lambda_c = 2.12\,\mu$m). We used NIRC2's narrow camera setting, which has a plate scale of 10 mas pixel^{-1}, to provide fine spatial sampling of the instrument point-spread function (PSF). Raw frames were processed by cleaning hot pixels, flat-fielding, subtracting background noise from the sky and instrument optics, and aligning and coadding the results. No off-axis sources were noticed in individual frames or the final processed image. Figure 2 shows the contrast levels generated by the observations. Our diffraction-limited images rule out the presence of companions down to $\Delta K' = 5.7, 7.1, 7.5$ mag at angular separations of $0\farcs25$, $0\farcs5$, and $1\farcs0$, respectively.

2.5.2. Lucky Imaging

Lucky imaging (LI) involves acquiring large numbers of observations with a rapid cadence. A subset of these images are then shifted and stacked in order to produce nearly-diffraction-limited images. GSC 03546-01452 was observed over 3 nights separated by 2 yr using FastCam (Oscoz et al. 2008) on the 1.5 m TCS telescope at Observatorio del Teide in Spain. The LI frames were acquired on 2010 October 9, 2011 August 25 and 2012 September 11 in the I band and spanning $\sim 21 \times 21$ arcsec^2 on sky.

The 2010 October 11 observing run had 100,000 frames with 50 ms per frame, the 2011 August 25 run had 60,000 frames with 60 ms per frame, and the 2012 September 11 run had 75,000 frames at 60 ms per frame. The data were processed using a custom IDL software pipeline. After identifying corrupted frames due to cosmic rays, electronic glitches, etc., the remaining frames are bias corrected and flat fielded.

Lucky image selection is applied using a variety of selection thresholds based on the brightest pixel (BP) method. This method involves selecting frames for the final combined LI image based on the BP in that frame. The selected BP must be below a specified brightness threshold to avoid selecting cosmic rays or other non-speckle features. As a further check, the BP must be consistent with the expected energy distribution from a diffraction speckle under the assumption of a diffraction-limited PSF. The BP's of each frame are then sorted from brightest to faintest, and the best $X\%$ are then shifted and added to generate a final combined image. Several values of X, the LI threshold, are tried until the best combined image is generated. The combined images using different LI thresholds are shown for each of the three observing runs in Figure 3. The 2012 September 11 run has a better quality image than the other two runs because of an instrument upgraded to a higher sensitivity CCD. The best LI threshold was determined to be 50%, which is what we used for the rest of the analysis. This results in a total exposure time for each of the final combined images from the three runs in order of date 2500, 1800, and 2250 s, respectively.

In Figure 4, we show the 3σ detectability curves computed out to $8''$ from GSC 03546-01452. We follow the same procedure as in Femenía et al. (2011) to compute these curves: at a given angular distance ρ from GSC 03546-01452, we identify all possible sets of small boxes of a size larger but comparable to the FWHM of the PSF (i.e., 5×5 pixel boxes). Only regions of the image showing structures easily recognizable as spikes due to diffraction of the telescope spider and/or artifacts on the read-out of the detector are ignored. For each of the valid boxes on the arc at angular distance ρ the standard deviation of the image pixels within the 5-pixel boxes is computed. The value assigned to the 3σ detectability curve at ρ is three times the mean value from the standard deviations of all the eligible boxes at ρ. This procedure, using each of the LI % thresholding values provides a detectability curve, while the envelope of all the family of curves for a given night yields the best possible detectability curve to be extracted from the whole data set.

Although there are no companions detected within $7''$, we do find a possible companion slightly outside this region at a separation of $7\farcs7$. This companion is significantly dimmer than GSC 03546-01452 with a $\Delta I \approx 7.9$ mag. This object was only detected in the 2010 October 11 and 2012 September 11 campaigns. The visual companion was not detected in the 2012

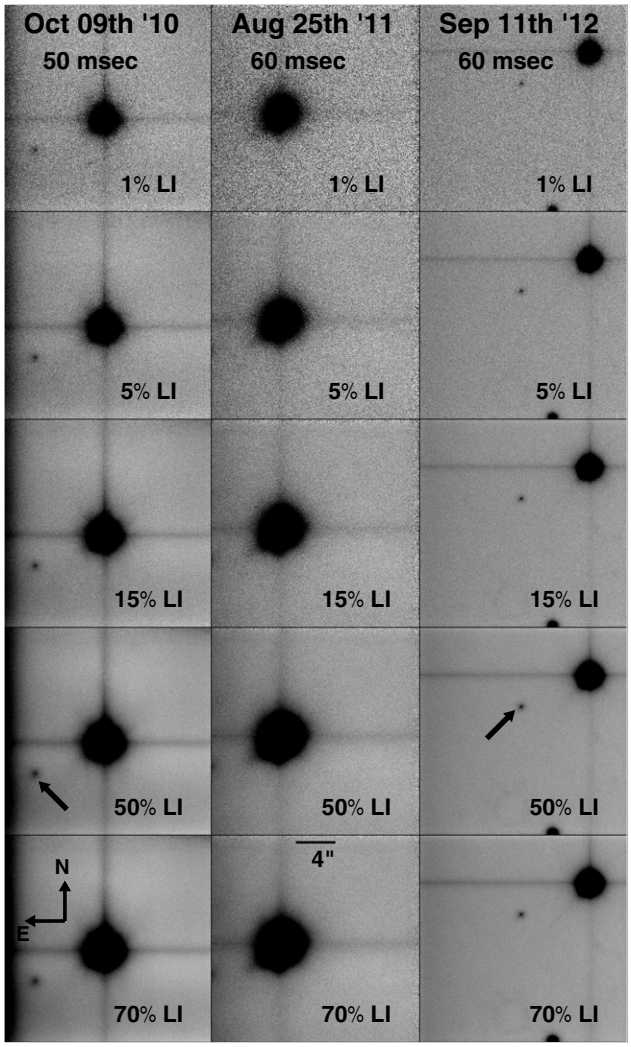

Figure 3. GSC 03546-01452 was observed on 2010 October 9, 2011 August 25, and 2012 September 11 with LI from the FastCam imager. The mosaic shows the final LI combined images from each run using different thresholds. LI detected a previously known visual companion 7.″7 away from GSC 03546-01452 (marked with an arrow) in the 2010 October 9 and 2012 September 11 runs. The companion was not detected on the 2011 August 25 night because it was not in the field of view of the camera. This visual companion has $\Delta I \approx 7.9$ mag. Further analysis showed that the companion is in fact a background star. For more details, see Section 3.5.

August 25 campaign due to the orientation of the camera on the sky. The possible companion can be seen in Figure 3. A discussion of the likelihood that this object is actually a bound companion to GSC 03546-01452 can be found in Section 3.5.

3. RESULTS

3.1. Host Star Characterization

3.1.1. Spectroscopic Analysis

The ARCES moderate resolution spectrum (Section 2.3) was analyzed by two independent analysis pipelines. We refer to these pipeline results as the "IAC" (Instituto de Astrofísica de Canarias) and "BPG" (Brazilian Participation Group) results. Briefly, both methods are based on the principals of Fe I and Fe II excitation and ionization equilibria. Both techniques employ the 2002 version of the MOOG code (Sneden 1973), but use different line lists, model atmosphere grids, equivalent width measurements, and convergence criteria. For a complete description of the analysis process, please refer to Wisniewski et al. (2012).

Our IAC analysis used 204 Fe I lines and 20 Fe II lines, and resulted in the following parameters: $T_{\rm eff} = 5502 \pm 100$, $\log g = 4.21 \pm 0.58$, and [Fe/H] $= +0.31 \pm 0.16$. The BPG analysis used 61 Fe I lines and 6 Fe II lines resulting in these parameters: $T_{\rm eff} = 5652 \pm 75$, $\log g = 4.46 \pm 0.16$, and [Fe/H] $= +0.44 \pm 0.10$. Since the values for both methods are consistent to within 1σ, they were combined using a weighted average as described in Wisniewski et al. (2012). This calculation resulted in the final spectroscopic parameter values of $T_{\rm eff} = 5598 \pm 63$, $\log g = 4.44 \pm 0.17$, and [Fe/H] $= +0.40 \pm 0.09$. These values are recorded in Table 3, and are used for the remaining analysis.

From these values of $T_{\rm eff}$, $\log g$, and [Fe/H] and their errors, and using the Torres et al. (2010) relations, including intrinsic scatter and the uncertainties in the polynomial coefficients and covariances, we find that the mean and rms of the mass and radius of the host are $M_* = 1.11 \pm 0.11\,M_\odot$ and $R_* = 1.06 \pm 0.23\,R_\odot$ The median and 68% confidence intervals are $M_* = 1.11^{+0.11}_{-0.10}\,M_\odot$ and $R_* = 1.03^{+0.26}_{-0.19}\,R_\odot$.

These spectroscopic values also allow us to transform the detection curves from the left panel of Figure 4 into upper limits on the mass of a possible stellar companion undetected at the 3σ level. We start by taking the spectroscopic $T_{\rm eff}$ from Table 3,

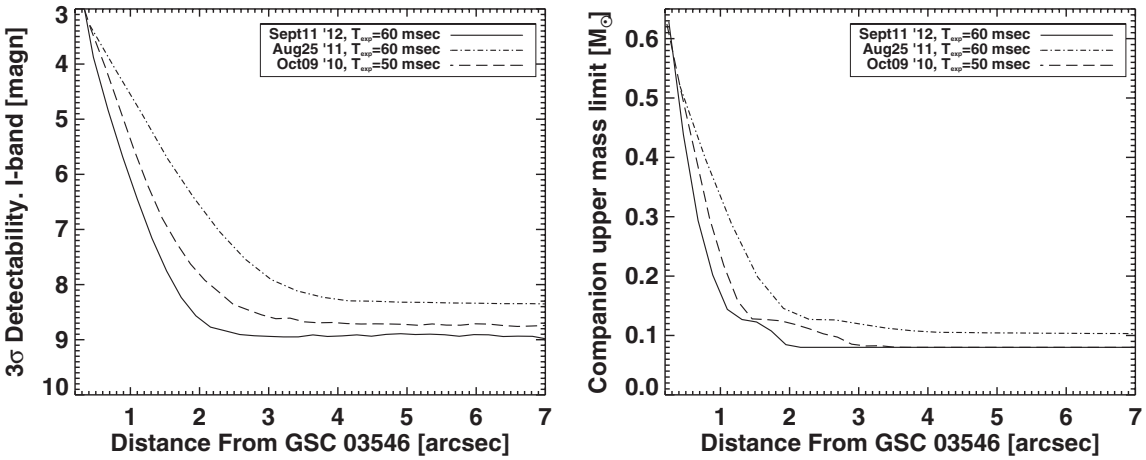

Figure 4. Left: 3σ detectability curves for LI from the FastCam imager. There was significant variation in the curves over the three runs. The best run can detect sources down to $\Delta I = 8.5$ beyond 2″. No source was detected within 7″ of GSC 03546-01452. Right: conversion of 3σ detectability curves for the three observing nights into mass sensitivities using empirical mass–luminosity relationships in the literature. See Section 3.5.

Table 3
Host Star Properties GSC 03546-01452

Parameter	Value	1σ Uncertainty	Source
GSC1.1 Name	3546-01452	···	Lasker et al. (2008)
GSC2.3 Name	N2EA000110	···	Lasker et al. (2008)
KIC Name	11022130	···	Brown et al. (2011)
2MASS Name	J19113252+4830436	···	Cutri et al. (2003)
α (J2000) (deg)	287.885735	0.″26	Lasker et al. (2008)
δ (J2000) (deg)	48.512117	0.″25	Lasker et al. (2008)
μ_α (mas yr^{-1})	−28.6	2.3	Zacharias et al. (2013)
μ_δ (mas yr^{-1})	−8.7	1.7	Zacharias et al. (2013)
$T_{\rm eff}$ (K)	5598	63	This work
log g (cgs)	4.44	0.17	This work
[Fe/H] (dex)	+0.40	0.09	This work
$v_{\rm mic}$ (km s^{-1})	0.38	0.17	This work
$v_{\rm rot} \sin i$ (km s^{-1})	<9.0	···	This work
$v_{\rm systemic}$ (km s^{-1})	−13.799	0.034	This work
A_V (mag)	0.1	0.1	This work
Distance (pc)	219	21	This work
M_* ($M_\odot$)	1.11	0.11	This work
R_* ($R_\odot$)	1.06	0.23	This work
galNUV	18.320	0.100	Morrissey et al. (2007)[a]
B	12.593	0.020	HAO (This work)[a]
V	11.799	0.010	Derived from HAO
R_C	11.335	0.012	Derived from HAO
I_C	10.967	0.012	Derived from HAO
SDSS u'	13.483	0.020	HAO (This work) [a]
SDSS g'	12.156	0.012	HAO (This work)[a]
SDSS r'	11.560	0.010	HAO (This work)[a]
SDSS i'	11.400	0.010	HAO (This work)[a]
2MASS J	10.46	0.030	Cutri et al. (2003)[a]
2MASS H	10.07	0.030	Cutri et al. (2003)[a]
2MASS K_S	10.010	0.03	Cutri et al. (2003)[a]
WISE1	12.650	0.023	Wright et al. (2010)[a]
WISE2	13.344	0.020	Wright et al. (2010)[a]
WISE3	15.181	0.032	Wright et al. (2010)[a]

Note. [a] These passbands were used to generate SED in Figure 5.

and using the tables from Mamajek (2010), we derive absolute V- and I-band magnitudes. We can apply this technique because GSC 03546-01452 has been identified as a main-sequence star by the log g measurement. The M_I and the 3σ detectability curves allow the construction of the M_I versus angular distance, ρ, from the central star. This curve provides an absolute upper I-band limit to any companion, which would also have to be a main-sequence star. From the M_V versus ρ curves we can use empirical mass–luminosity relationships (Henry et al. 1999; Delfosse et al. 2000; Henry 2004; Xia et al. 2008; Xia & Fu 2010) to derive the upper mass limit. These constraints are plotted for all three observation nights in the right panel of Figure 4.

3.1.2. Photometric Analysis

We corroborated the spectroscopic results with a series of photometric tests, including determining the RPM-J statistic from Collier Cameron et al. (2007). For GSC 03546-01452, the RPM-J value was 2.31 and its $(J-H)$ 2MASS color was 0.387, results that are consistent with GSC 03546-01452 being a dwarf.

We also constructed a spectral energy diagram (SED) of GSC 03546-01452 using the *Galaxy Evolution Explorer* (*GALEX*) NUV filter (Morrissey et al. 2007); Johnson B and SDSS u',g',r',i' observations from HAO; 2MASS J, H, and K (Cutri et al. 2003); and *WISE1*, *WISE2*, and *WISE3* (Wright et al. 2010). A summary of the photometric values are presented in Table 3. We used the NextGen model atmosphere grid (Hauschildt et al. 1999) to construct theoretical SEDs. These models were fixed by the spectroscopic values for $T_{\rm Eff}$, log g, and [Fe/H] described in Section 3.1.1; the reddening was constrained by the Schlegel et al. (1998) dust maps in the direction of $(l, b) = (79.^\circ339029, 16.^\circ853379)$ to be less than $A_V = 0.213$. The resulting fit to the photometry is shown in Figure 5. The best fitting model has a reduced χ^2 of 3.91, a negligible reddening of $A_V = 0.1 \pm 0.1$, and a distance of 219 ± 21 pc. There appears to be a slight UV excess, which may be the result of modest stellar activity.

3.1.3. Evolutionary Status and Galactic Population

Using the spectroscopic host star parameters and the mass and radius derived from the Torres et al. (2010) relations, GSC 03546-01452 can be placed onto an evolutionary track. We use the Yonsei-Yale ("Y2") model tracks from Demarque et al. (2004 and references therein), and select the track corresponding to 1.11 $M_\odot$ with a [Fe/H] = +0.40. Figure 6 shows this track with stellar ages marked as blue dots on the track. The dashed lines show tracks for the same metallicity, but for $\pm 0.11\ M_\odot$, which is the 1σ uncertainty on our mass estimate. The gray area shows the region that this family of tracks occupies. The red point shows GSC 03546-01452 with 1σ error bars. From the error bars in log g and $T_{\rm eff}$ in Figure 6, we can constrain the age

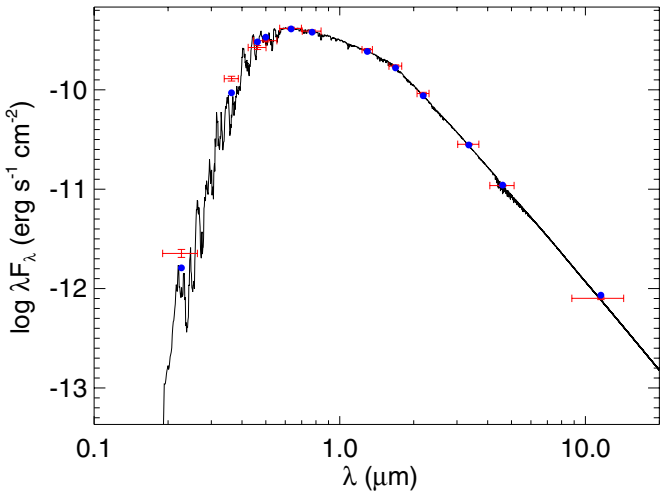

Figure 5. The spectral energy diagram (SED) for GSC 03546-01452. The black line shows the best fit NextGen model compared to the observed flux in the photometric passbands from Table 3 (red crosses). The horizontal bars are the approximate passband width for each filter, while the vertical bar is the error in the flux. The blue circles are the expected flux values from the model. The best fit model is fixed to the spectroscopically determined $T_{\rm eff}$, log g, and [Fe/H] and allowed A_V to float. The optical and infrared fit well, but there is a significant excess of flux in the *GALEX* NUV passband.

(A color version of this figure is available in the online journal.)

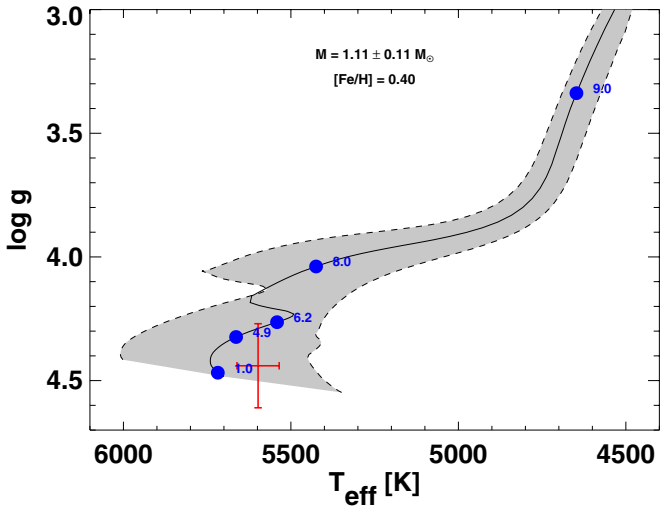

Figure 6. The black line represents the best fit Yonsei-Yale evolutionary track for a 1.1 $M_\odot$ star with a [Fe/H] of +0.40 (Demarque et al. 2004). The gray area denotes the 1σ deviation from that track. Ages along the track are denoted by blue dots for 1.0, 4.7, 6.4, 8.0, and 9.0 Gyr. The red cross denotes the location of GSC 03546-01452 on this diagram with the spectroscopic uncertainties.

(A color version of this figure is available in the online journal.)

of GSC 03546-01452 to being less than approximately 6 Gyr old.

We can determine the Galactic population membership of GSC 03546-01452 by using the absolute systemic RV $= -13.799 \pm 0.128$ km s^{-1} (where the 0.128 km s^{-1} is a conservative estimate of the systematic error from the comparison with RV standard stars), the proper motions from UCAC4 (Zacharias et al. 2013; $\mu = -28.6 \pm 2.3, -8.7 \pm 1.7$ mas yr^{-1}), and the distance from Table 3 (219 ± 21 pc). We find $(U, V, W) = (24.0 \pm 2.5, -10.1 \pm 1.3, 25.6 \pm 3.1)$ km s^{-1}. This velocity is consistent with membership in the thin disk according to the criteria of Bensby et al. (2003). The space motion velocities were determined using a modification of the IDL routine `GAL_UVW`, which is ultimately based on the method of Johnson & Soderblom (1987). We adopt the correction for the Sun's motion with respect to the local standard of rest from Coşkunoğlu et al. (2011), and choose a right-handed coordinate system such that positive U is toward the Galactic Center.

Table 4
Properties for MARVELS-6b

Parameter	Units	Value
T_C	BJD$_{\rm TDB}$ − 2450000	$5023.377^{+0.10}_{-0.099}$
P	Period (days)	$47.8929^{+0.0063}_{-0.0062}$
e	Eccentricity	$0.1442^{+0.0078}_{-0.0073}$
ω	Argument of periastron (radians)	$1.998^{+0.064}_{-0.061}$
K	RV semi-amplitude (m s^{-1})	1644^{+12}_{-13}
$\gamma_{\rm TNG}$	TNG systemic velocity (m s^{-1})	724 ± 15
dv/dt	RV slope (m s^{-1} day^{-1})	0.180 ± 0.053
$\gamma_{\rm APO}$	APO systemic velocity (m s^{-1})	1058^{+17}_{-16}
$e\cos(\omega)$	...	$-0.0597^{+0.0071}_{-0.0070}$
$e\sin(\omega)$	...	$0.1312^{+0.0093}_{-0.0092}$
T_P	BJD$_{\rm TDB}$ − 2450000	$5025.81^{+0.46}_{-0.44}$
$M_b \sin i$	Minimum mass ($M_{\rm Jup}$)	$31.7^{+2.0}_{-2.0}$

3.2. Companion Orbital Analysis

The orbital parameters of MARVELS-6b were derived using the radial velocity data from both the MARVELS and the SARG spectrographs. The orbital fit was created using the EXOFAST[27] code (Eastman et al. 2013), which allowed us to determine the usual Keplerian orbital elements shown in Table 4.

The first step in the process was to perform independent fits to both the MARVELS and SARG data points. Both data sets had error bars that were too large based on the χ^2 of their fits, so we re-scaled them to force the probability that the χ^2 is greater than or equal to the measured χ^2, i.e., $P(\chi^2), = 0.5$. The MARVELS error bars were scaled by a factor of 0.579, and the SARG error bars were scaled by a factor of 0.222. The error bars in Table 1 include these scaling factors.

Once the error bars were scaled, the two data sets were combined. The final combined radial velocity curve was then run through EXOFAST which is a Markov Chain Monte Carlo (MCMC) based IDL software suite. The basic algorithms of this software follow the work of Ford (2006). The results of the combined fit are listed in Table 4, and the best-fit model is shown in Figures 7 and 8.

The radial velocity measurements from both MARVELS and SARG are relative radial velocities. As part of the fitting process, EXOFAST fits and subtracts arbitrary zero points for each data set simultaneously. These zero points are recorded in Table 4. These offsets are based on arbitrary zero-points, and should not be confused with the true systemic velocity of the host system -13.799 ± 0.128 km s^{-1}.

The systemic velocity of GSC 03546-01452 was derived by taking the orbital solution from EXOFAST for the combined relative radial velocity data set and applying it to the SARG/TNG absolute velocity data set (Table 2.). This calculation was performed by using the MPFIT Levenberg–Marquardt non-linear least squares fitting algorithm in IDL (Markwardt 2009). A Keplerian model was fit to the SARG/TNG radial

[27] http://astroutils.astronomy.ohio-state.edu/exofast/

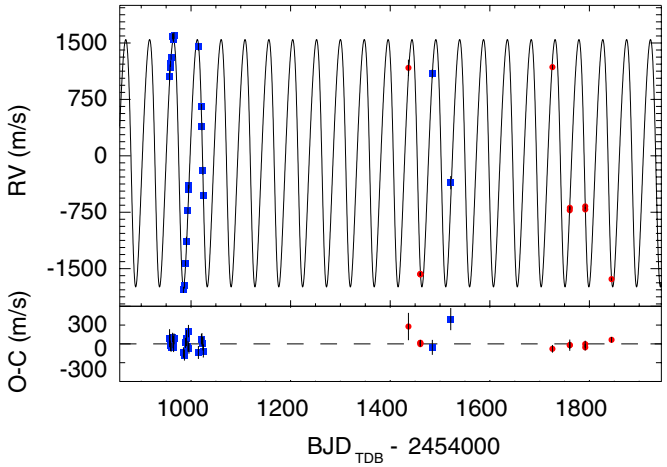

Figure 7. All the radial velocity points from both the MARVELS Survey (blue squares) and TNG/SARG follow-up spectroscopy (red circles). The final best fit for a $M_b \sin i = 31.7 \pm 2.0\ M_{\rm Jup}$ companion to GSC 03546-01452 (Table 4) is shown with the associated O-C diagram. The observation data points start at BJD = 2454956.916 (2009 May 5). There is a slight residual linear slope (0.180 m s^{-1} day^{-1}) after removing the companion orbit.

(A color version of this figure is available in the online journal.)

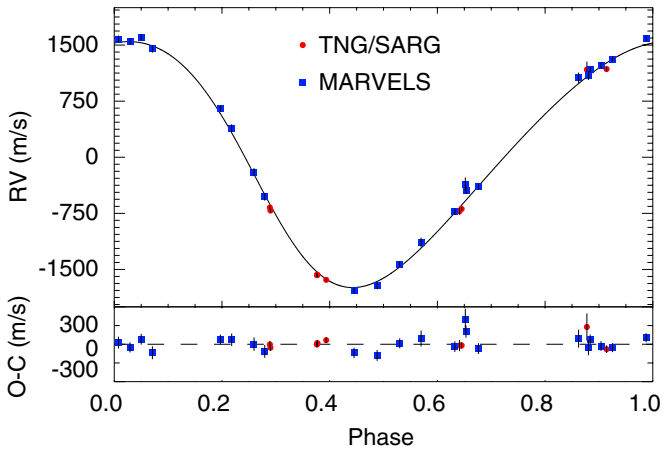

Figure 8. The phased final RV curve including both the MARVELS Survey (blue squares) and the TNG/SARG observations (red circles). The final best fit for a $M_b \sin i = 31.7 \pm 2.0\ M_{\rm Jup}$ companion to GSC 03546-01452 (Table 4), is shown with the associated O-C diagram.

(A color version of this figure is available in the online journal.)

velocity points, holding P, e, ω, K, and T_P fixed while allowing γ to float; the results are presented in Table 3.

3.3. Companion Mass

3.3.1. Mass Functions of Secondary

The mass function ($\mathcal{M}_b$) is the only property of a single-lined radial velocity companion that we can derive that is independent of the properties of the primary. Using the MCMC chain from the joint RV fit, we can derive $\mathcal{M}_b$ of the companion,

$$\mathcal{M}_b \equiv \frac{(M_b \sin i)^3}{(M_* + M_b)^2} = K^3(1-e^2)^{3/2}\frac{P}{2\pi G} = (2.136 \pm 0.049) \times 10^{-5}\ M_\odot, \quad (1)$$

where the uncertainty is essentially dominated by the uncertainty in K, such that $\sigma_{\mathcal{M}_b}/\mathcal{M}_b \sim 3(\sigma_K/K) = 3 \times 0.8\% \sim 2.4\%$.

3.3.2. Minimum Mass and Mass Ratio

In order to determine the mass or mass ratio of the secondary, we must estimate the mass of the primary as well as the inclination of the secondary.

To estimate the mass and radius of the primary, we proceed as follows. For each link in the MCMC chain from the joint RV fit, we draw a value of $T_{\rm eff}$, $\log g$, and [Fe/H] for the primary from Gaussian distributions, with means and dispersions given in Table 3. We then use the Torres et al. (2010) relations to estimate the mass M_* and radius R_* of the primary, including the intrinsic scatter in these relations.

The minimum mass (i.e., M_b if $\sin i = 1$) and minimum mass ratio of the secondary are:

$$M_{b,\rm min} = 31.7 \pm 2.0\ M_{\rm Jup} = 0.0303 \pm 0.0020\ M_\odot, \quad q_{\rm min} = 0.02733 \pm 0.00092. \quad (2)$$

The uncertainties in these estimates are almost entirely explained by the uncertainties in the mass of the primary: $\sigma_{M_b}/M_b \sim (2/3)(\sigma_{M_*}/M_*) = (2/3) \times 9.7\% \sim 6.5\%$, close to the uncertainty in $M_{b,\rm min}$ above (6.4%), and $\sigma_q/q \sim (1/3)(\sigma_{M_*}/M_*) \sim (1/3) \times 9.7\% \sim 3.2\%$, close to the uncertainty in q (3.4%).

3.3.3. A Posteriori Distributions of the True Mass

The *a posteriori* distribution of the true mass of the companions given our measurements depends on our prior distribution for the mass of the companion, which is roughly equivalent to our prior on the mass ratio.

If we assume a prior that is uniform in the logarithm of the true mass of the companion, then the posterior distribution of $\cos i$ will be uniform. More generally, for other priors, $\cos i$ is not uniformly distributed. We adopt priors of the form

$$\frac{dN}{dq} \propto q^\alpha, \quad (3)$$

where q is the mass ratio between the companion and the primary, and $\alpha = -1$ for the uniform logarithmic prior discussed above. To include this prior, for each link of the MCMC chain we draw a value of $\cos i$ from a uniform distribution, but then weight the resulting values of the derived parameters for that link (i.e., the companion mass m) by $q^{\alpha+1}$.

For $\alpha > 0$, the *a posteriori* distribution does not converge. However, we can rule out equal mass ratio companions by the lack of a second set of spectral lines. We therefore assume that the mass ratio cannot be greater than unity; i.e., we give zero weight to inclinations such that $q > 1$. In doing so, we implicitly assume that the companion is not a stellar remnant.

Figures 9 shows the resulting cumulative *a posteriori* distributions of the true mass of the companion for $\alpha = -1$ (uniform logarithmic prior on q), $\alpha = 0$ (uniform linear prior), and $\alpha = 1$. For $\alpha = -1$ and $\alpha = 0$, the inferred median masses are $\sim$37 $M_{\rm Jup}$ and $\sim$45 $M_{\rm Jup}$, respectively. For these priors, we conclude that the companion has a mass below the hydrogen burning limit and thus is a *bona fide* brown dwarf at 90% and 72% confidence, respectively. For $\alpha = 1$, the median mass is 172 $M_{\rm Jup}$ or $\sim$0.16 $M_\odot$, firmly within the stellar regime. Indeed, for this prior, there is only a $\sim$32% probability that the companion is a brown dwarf. However, this conclusion is sensitive to the precise form for our constraint that $q \leqslant 1$. With a more careful analysis it may be possible to rule out a wider range of companion masses based on the lack of evidence for a second set of spectral lines. Furthermore, there is little evidence that the mass function of companions to solar type stars is rising as

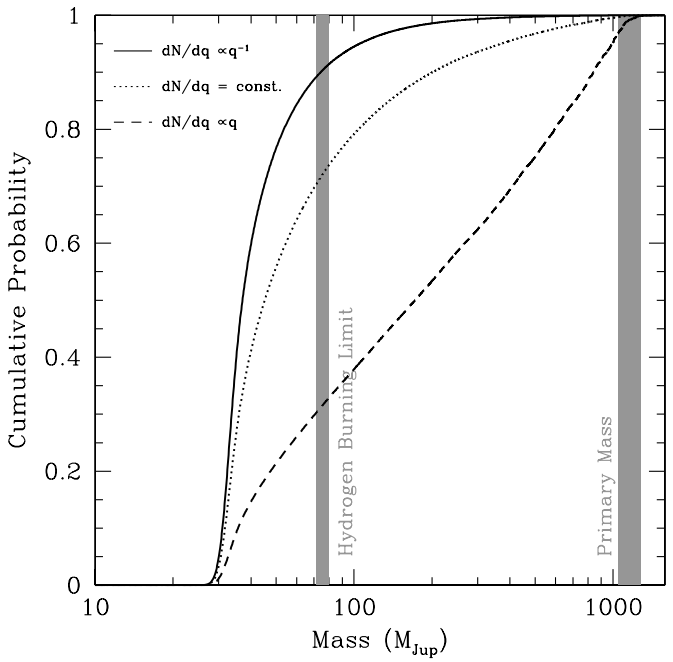

Figure 9. The cumulative *a posteriori* probability of the true mass of the secondary, for three different priors on the companion mass ratio, $dN/dq \propto q^{\alpha}$, with $\alpha = -1$ (solid), $\alpha = 0$ (dotted) and $\alpha = 1$ (dashed). Also indicated are the mass of the primary with uncertainty and the hydrogen burning limit, both denoted by shading. For $\alpha = -1$ and $\alpha = 0$, the inferred median masses are $\sim$37 $M_{\rm Jup}$ and $\sim$45 $M_{\rm Jup}$, respectively. For these priors, we conclude that the companion has a mass below the hydrogen burning limit and thus is a *bona fide* brown dwarf at 90% and 72% confidence, respectively. For $\alpha = 1$, the median mass is 172 $M_{\rm Jup}$ or $\sim$0.16 $M_{\odot}$, firmly within the stellar regime. However, it is unlikely that $\alpha > 0$ in this mass regime.

steeply as $\alpha = 1$ for minimum masses around 30 $M_{\rm Jup}$ (Grether & Lineweaver 2006).

We conclude that the companion to GSC 03546-01452 is most likely a brown dwarf. However, we cannot definitively exclude that it is, in fact, a low-mass stellar companion seen at low inclination.

3.4. Time-series Photometric Analysis

3.4.1. Summary of Datasets

The SuperWASP photometric dataset for GSC 03546-01452 consists of 8823 points spanning just over 4 yr from HJD$'$ = 3128 to 4690 (where HJD$'$ $\equiv$ HJD $-$ 2450000). The full, detrended SuperWASP dataset has a relatively high weighted rms of 1.8% and exhibits evidence for systematics. The distribution of residuals from the weighted mean is asymmetric and non-Gaussian, showing long tails containing a much larger number of $>3\sigma$ outliers than would be expected for a normally-distributed population. We therefore cleaned the SuperWASP data as follows. We first add a trial systematic fractional error in quadrature to the photon noise uncertainties $\sigma_{\rm sys}$. We then compute the error-weighted mean flux, and determine and reject the largest error-normalized outlier from the mean flux. We then recompute the mean flux and scale the uncertainties by a constant factor r to force $\chi^2/{\rm dof} = 1$. We iterate this procedure until no more $>4\sigma$ outliers remain. We then repeat the entire procedure to determine the value of $\sigma_{\rm sys}$ that results in a distribution of normalized residuals that has the smallest rms from the Gaussian expectation. Although 4σ is a slightly larger deviation than we would expect based on the final number of points, we adopt this conservative threshold in order to avoid removing a potential transit signal. We adopt $r = 0.60$ and $\sigma_{\rm sys} = 0.011$. The cleaned light curve has 8635 data points with an rms of 1.5% and $\chi^2/{\rm dof} = 1$ (by design).

The Allegheny photometric dataset consists of 3990 points spanning roughly a year and a half from HJD$'$ = 5341 to 5884. The weighted rms of the raw light curve is 0.63%. There is mild evidence for systematics errors in this dataset, and thus we repeat the identical procedure as with the SuperWASP data. We choose a more conservative 6σ cut, given the better precision of the Allegheny observations, to prevent us from removing real transit-like variability. We adopt $r = 1.04$ and $\sigma_{\rm sys} = 0.0028$, with a final rms of 0.4% from 3983 data points.

While continuous variability will not be removed by our procedure, variability in the form of a small number of highly-discrepant points will be masked. This possibility is particularly relevant for transit signatures. Given the typical uncertainties of $\sim$0.4% for that data set, we do not expect our cleaning procedure to remove outliers that differ by less than $\sim$2.4% from the mean, roughly corresponding to the typical depth for a transit of a $\sim$1.5 $R_{\rm Jup}$ companion given the primary radius of $\sim$1.03 $R_{\odot}$.

Finally, we combine all the relative photometry after normalizing each individual data set by its mean weighted flux. Figure 10 shows the combined data set, which consists of 12,618 data points spanning roughly 7.6 yr from HJD$'$ = 3128 to 5884. The weighted rms is 0.66%. The resulting light curve is constant to within the uncertainties over the entire time span. Because the individual data sets sample disjoint times and are not relative to a common set of reference stars, our procedure of normalizing each data set by its mean flux will remove variations on the longest timescales.

3.4.2. Search for Variability

We ran a Lomb–Scargle periodogram on the full photometric dataset, testing periods between 1 and 10^3 days. The resulting periodogram shown in Figure 11 does not exhibit any strong peaks. The maximum fitted amplitude over this range is $\sim$0.1%. The inset presents the periodogram of the combined data set for periods within $\sim$10 days of the period of the companion. The individual periodograms for the SuperWASP and Allegheny data are also shown. While the SuperWASP data display a local peak at the period of the companion, this feature is not corroborated by the Allegheny data. Although this difference could in principle arise from real variability that is present in the SuperWASP data, but not in the Allegheny data (i.e., evolving spots), given the higher precision of the Allegheny data, we believe it is more likely that the peak in the SuperWASP periodogram is due to low-level systematics in the form of residual correlations on a range of time scales.

Figure 12 shows the combined light curve, folded at the median period and time of conjunction of the companion ($P = 47.8929 \pm 0.0063$ and $T_C = 5023.377$) and binned 0.05 in phase. The weighted rms of the binned light curve is $\sim$0.041%. Although the variations are larger than expected from a constant light curve based on the uncertainties ($\chi^2/{\rm dof} \sim 2.6$), we again suspect that these are due to systematic errors in the relative photometry. In particular, the folded, binned Allegheny light curve shows a somewhat lower rms of $\sim$0.016%, and is more consistent with a constant flux with a $\chi^2/{\rm dof} = 0.4$.

We conclude that there is no strong evidence for variability of GSC 03546-01452 on any time scale we probe. We can robustly constrain the amplitude of any persistent periodic variability to be less than $\lesssim$0.1% over timescales of $\lesssim$3 yr, and we can

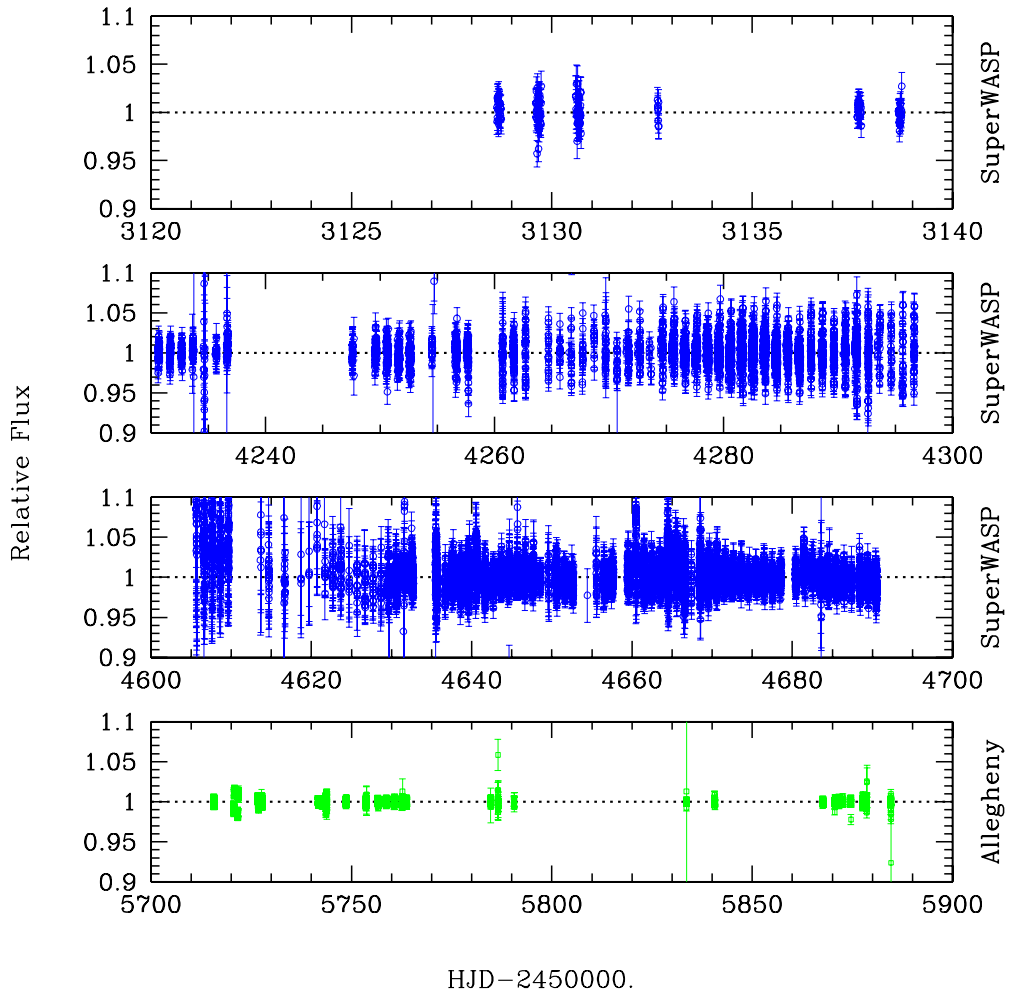

Figure 10. Cleaned broad band relative photometry of GSC 03546-01452 from SuperWASP (blue) and Allegheny (green) as a function of date.
(A color version and FITS images of this figure are available in the online journal.)

constrain the amplitude of persistent photometric variability at the period of the companion to $\lesssim$0.02%.

3.4.3. Excluding Transits of the Secondary

For a uniform distribution in $\cos i$ (corresponding to a prior that is uniform in the logarithm of the mass), the secondary transit probability is ∼1.8%. The duration for a central transit is $\sim R_* P/(\pi a) \sim 6.6$ hr, and the depth for a Jupiter-radius body is $\delta \sim (R_b/R_*)^2 = 1.0\%(R_b/R_{\rm Jup})^2$, where R_b is the radius of the companion, and we have adopted the median value for the primary radius of $R_* = 1.03\ R_\odot$. Thus, the expected S/N of a transit in the combined photometric dataset assuming uniform phase coverage is

$$\mathrm{S/N} \sim N^{1/2} \left(\frac{R_*}{\pi a}\right)^{1/2} \frac{\delta}{\sigma} \sim 13 \left(\frac{R_b}{R_{\rm Jup}}\right)^2, \qquad (4)$$

where $N = 12618$ is the number of data points and $\sigma \sim 0.66\%$ is the rms of the combined light curve. Thus we would expect to be able to robustly detect or exclude transits from companions with radii as small as ∼0.9 $R_{\rm Jup}$ at 10σ if the transit phase is well covered by the photometric data. However, given the long period of the companion, uniform phase coverage is not necessarily a good approximation.

Therefore, in order to account for the actual sampling of the photometric data, we perform a quantitative search for transit signals using a modified Monte Carlo method. This method is similar to that described in Fleming et al. (2012). We briefly review the details here. We start with the distributions of the relevant radial velocity fit parameters: the period P, semiamplitude K, eccentricity e, and time of conjunction T_C. These are obtained from the MCMC chain determined by fitting of the joint radial velocity data set as described in 3.2. For each link in this MCMC chain, we also draw values for $T_{\rm eff}$, $\log g$, and [Fe/H] for the primary from Gaussian distributions, with means and dispersions given in Table 3. We then use the Torres et al. (2010) relations to estimate the mass M_* and radius R_* of the primary, including the intrinsic scatter in these relations. We then draw a value of $\cos i$ from a uniform distribution, assuming a prior on the companion mass M_b that is uniform in $\log M_b$. The values of P, K, e, M_*, R_* and i are then used to determine the secondary mass M_b, semimajor axis a, and impact parameter of the secondary orbit $b \equiv a \cos i / R_*$. From the impact parameter, we determine if the companion transits ($b \leqslant 1$), and if so, we determine the properties of the light curve using the routines of Mandel & Agol (2002) for a given companion radius R_b. We assume quadratic limb darkening, adopting coefficients appropriate for the R band from Claret & Hauschildt (2003), assuming solar metallicity and the central values of $T_{\rm eff}$ and $\log g$ listed in Table 3. Finally, we fit the predicted transit light curve to the combined photometric data, and compute the $\Delta\chi^2$ between the constant flux fit and the

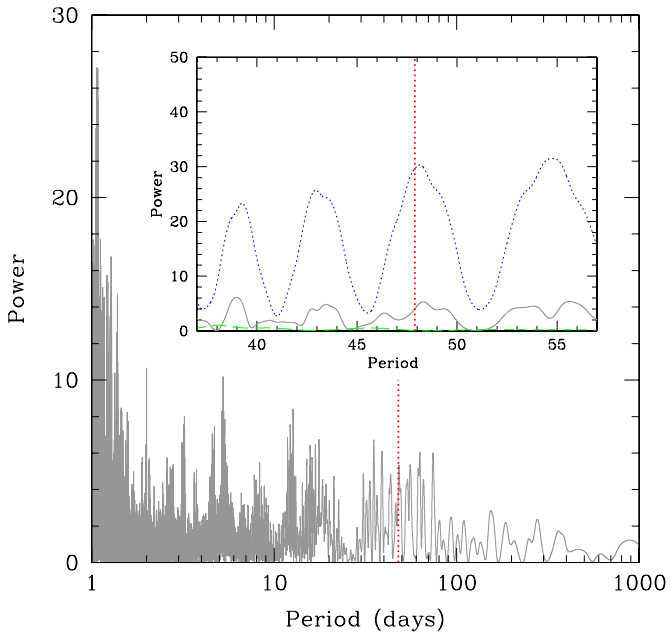

Figure 11. Lomb–Scargle periodogram of the combined photometric data. While a large number of peaks are visible, we do not regard any of them as significant. In particular, while there is a local peak at the period of the secondary (vertical red dotted line), this peak arises from the SuperWASP data alone, and is not confirmed by the Allegheny data. This result is demonstrated in the inset, which shows the combined periodogram near the period of the companion (gray solid), the periodogram of the SuperWASP data alone (blue dotted), and Allegheny alone (blue long dashed).

(A color version of this figure is available in the online journal.)

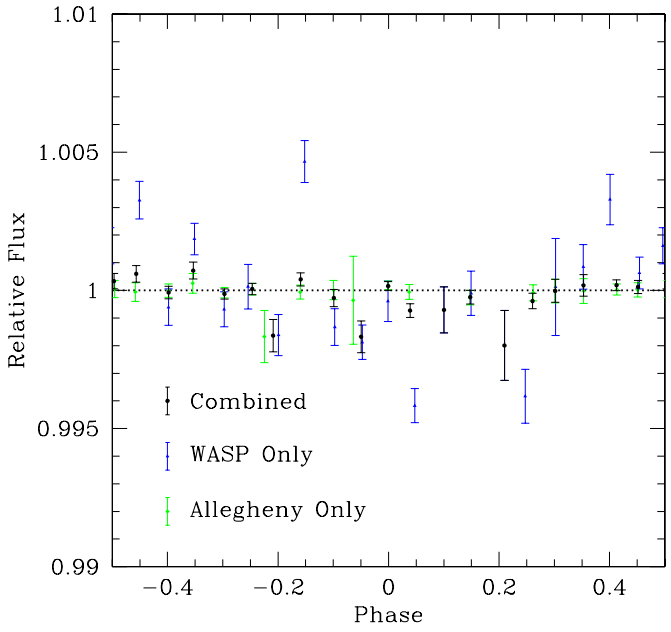

Figure 12. Relative photometry folded at the period of secondary and binned 0.05 in phase. Phase zero corresponds to the expected time of conjunction (and so of transits for the appropriate inclinations). The black points are the combined data, the blue are SuperWASP, and the green are Allegheny.

(A color version of this figure is available in the online journal.)

transit model. We perform this calculation for every step in the Markov Chain, and finally repeat this procedure for a range of companion radii.

We find that a best-fit transit model has $\Delta\chi^2 = -9.0$ relative to a constant fit. We do not consider this result to be significant,

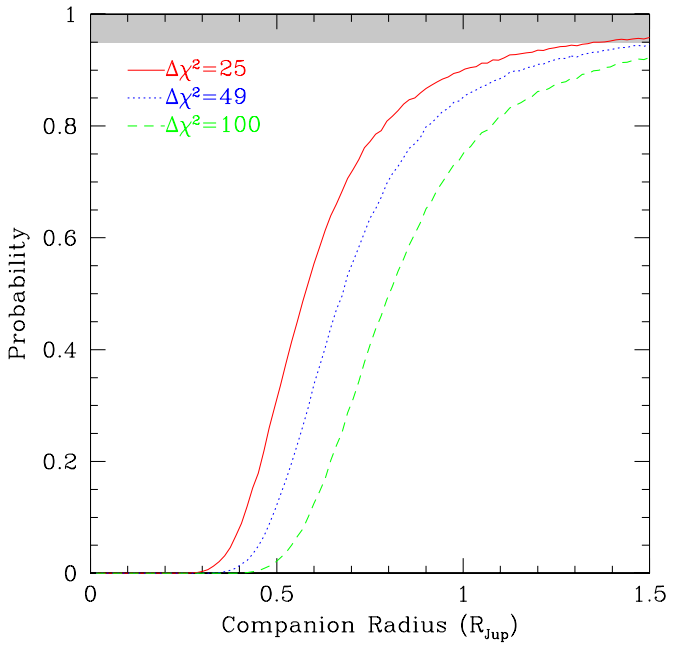

Figure 13. Probability that transits of a companion are excluded at levels of $\Delta\chi^2 = 25, 49, 100$ based on the analysis of the combined SuperWASP and Allegheny photometric data sets, as a function of the radius of the companion. The gray region represents the 95% confidence level. Only the $\Delta\chi^2 = 25$ model crosses into the gray region, thus we cannot rule out a possible transiting companion even with an unphysically large radii $R_b \gtrsim 1.5\ R_{\rm Jup}$ at the 95% level.

(A color version of this figure is available in the online journal.)

as we find a larger improvement $\Delta\chi^2 = -28.1$ when we consider signals with the same ephemeris and shape as transits, but corresponding to positive deviations (i.e., "anti-transits," see Burke et al. 2006). Although formally statistically significant, both the transit and anti-transit signals are likely caused by residual systematics in the cleaned photometric data set, and thus we conclude there is no evidence for a transit signal in the photometric data.

This procedure can be used to determine the confidence with which we can rule out transits of a companion with a given radius. Specifically, the confidence with which we can exclude a companion with a given R_b is simply the fraction of the steps in the Markov Chain where the companion transits, which produces a transit with a $\Delta\chi^2$ relative to the constant fit that is greater than some value of $\Delta\chi^2$. We consider three different thresholds of $\Delta\chi^2 = 25$, 49, and 100. The resulting cumulative probability distributions are shown in Figure 13. Given the values of $\Delta\chi^2$ found for anti-transits, we conservatively consider thresholds of $\Delta\chi^2 \gtrsim 49$ to be robust. For this value, we can exclude companions with $R_b \gtrsim 0.7\ R_{\rm Jup}$ with 50% confidence (i.e., for 50% of the trials), and companions with $R_b \gtrsim 1.2 R_J$ with 90% confidence. However, there is a long tail toward large companion radii, arising from the conflation of the long period of the companion, uncertainties in the ephemeris, and imperfect phase coverage. Therefore, we are unable to exclude transits at >95% confidence even for $R_b \gtrsim 1.5$. For the minimum companion mass of $\sim$32 $M_{\rm Jup}$, Baraffe et al. (2003) predict radii of $\sim$0.9–1 $R_{\rm Jup}$ for ages between 0.5 and 5 Gyr. Therefore, we cannot definitively exclude the possibility that the companion transits.

As discussed above, our 6σ clipping procedure would in principle remove $\gtrsim$2.4% transit signatures from the Allegheny

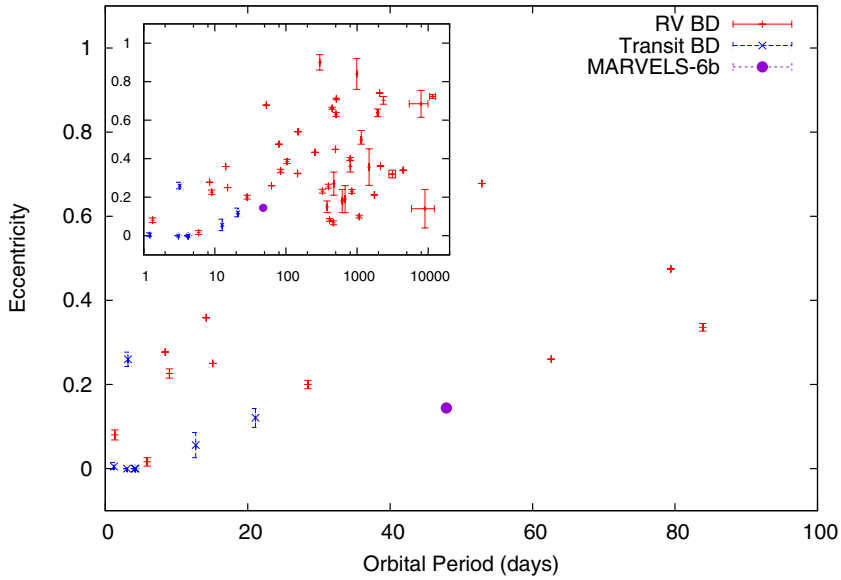

Figure 14. Orbital period and eccentricity of MARVELS-6b compared to a subset of literature brown dwarfs found through transit or radial velocity that occupy the period range of 0–100 days. The literature brown dwarfs are from the catalog of Ma & Ge (2013). MARVELS-6b occupies an empty part of orbital period/eccentricity plane. Inset: the full brown dwarf catalog extending out to much larger periods.

(A color version of this figure is available in the online journal.)

dataset arising from a large $R_b \gtrsim 1.5\ R_{\rm Jup}$ companion. We therefore repeated the transit search on the Allegheny dataset with 10σ clipping, but again find no significant transits.

3.5. LI Tertiary Companion

As discussed in Section 2.5.2, a possible tertiary companion was detected at 7.″7 from GSC 03546-01452 (see Figure 3). The possible tertiary companion has $\Delta I \approx 7.9$ mag, and at the measured distance to the host star in Table 3 places the companion at a projected distance of 1686 AU from the host star.

This possible tertiary companion can be found in both the 2MASS (Cutri et al. 2003) and Kepler Input Catalog (KIC; Brown et al. 2011). The KIC IDs of the primary and possible tertiary are 11022130 and 11022139, respectively. The first blow to the hypothesis that this is a bound system is found in the KIC itself. The KIC gives the following stellar parameter estimates for the possible tertiary $T_{\rm eff} = 5919$, $\log g = 4.361$, and $A_V = 0.515$. Comparing these values to the spectroscopic values determined for GSC 03546-01452 in Table 3, it is clear that these two objects cannot be bound, and have a ΔI of $\approx$7.9 mag; because two G dwarfs should have approximately the same magnitude. However, the tertiary is faint ($J = 16.272$), and the KIC spectroscopic determinations are photometric in nature, so we considered the possibility that the KIC parameters were incorrect.

GSC 03546-01452 has a measured proper motion from the UCAC4 catalog (Zacharias et al. 2013) of $\mu_\alpha = -28.6 \pm 2.3$ mas yr^{-1} and $\mu_\delta = -8.7 \pm 1.7$ mas yr^{-1} (see Table 3). This motion is significant given the plate scale of the LI images $\approx$42.56 mas pixel^{-1}, which, given our 2 yr baseline for observations, should be sufficient to test whether this is a bound system. Table 5 gives the difference in position between the GSC 03546-01452 and the possible tertiary in RAcos(DEC) and DEC for both LI observations. The two points are distinct to the 2σ level. We also have observations of both sources in 2MASS; although the astrometric position measurement is significantly worse, the 12 yr baseline between 2MASS and the 2012 observation compensates for the lower accuracy. These points are also distinct to the 2σ level. Given both the astrometric and photometric data, the hypothesis that this is a bound system is very unlikely.

Table 5
Difference in Position of GSC 03546-01452 versus Possible Tertiary

Year Observed	$\Delta\alpha\cos(\delta)$ (arcsec)	Error (arcsec)	$\Delta\delta$ (arcsec)	Error (arcsec)	Source
2012	7.232	0.049	−3.026	0.043	Lucky
2010	7.270	0.023	−3.163	0.018	Lucky
2000	6.86	0.11	−3.39	0.12	2MASS

4. DISCUSSION

Based on the derived spectroscopic parameters for the host star and the results discussed in Section 3.3.3, it is highly likely that MARVELS-6b is a BD companion to GSC 03546-01452 assuming a logarithmic or linear prior on the distribution of mass ratios. Working with the minimum mass for MARVELS-6b of $31.7 \pm 2.0\ M_{\rm Jup}$, we can compare it to the current distribution of masses in the literature. Grether & Lineweaver (2006) investigated the mass function of both stellar and planetary companions and found that they both decreased by a substantial fraction as they approached the minimum of the BD desert. In the case of the stellar mass function, it dropped by two orders of magnitude from the $1\ M_\odot$ to the middle of the BD desert. On the planetary mass side, it rises one order of magnitude as one progress away from the BD desert and toward lower mass planets.

MARVELS-6b is interesting because its minimum mass, $31.7 \pm 2.0\ M_{\rm Jup}$, lies at the very bottom of the two distributions. Grether & Lineweaver (2006) define their mass functions as the number of companions per unit interval in log mass, and find the minimum of the distributions to be at $31^{+25}_{-18}\ M_{\rm Jup}$. In order to better understand this minimum, it is necessary to increase the number of objects (or place tighter constraints by non-detections)

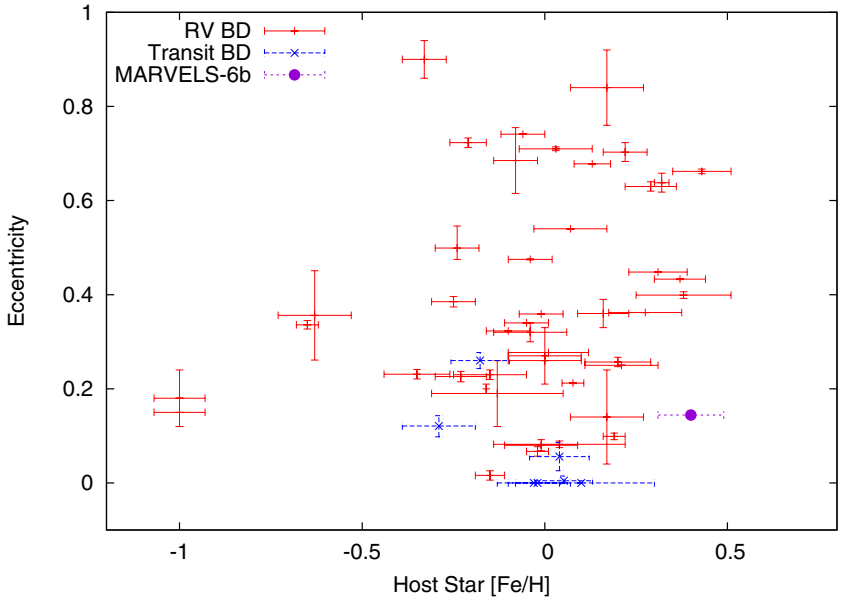

Figure 15. The host metallicity and orbital eccentricity of MARVELS-6b compared to the literature brown dwarfs from the catalog of Ma & Ge (2013). MARVELS-6b has a relatively low eccentricity and its host star has a quite high [Fe/H].
(A color version of this figure is available in the online journal.)

in this region of the mass function, and MARVELS-6b takes us one step closer to that goal.

MARVELS-6b stands out in respect to other brown dwarfs in two significant ways. First, it has a relatively low eccentricity, 0.1442, given its moderately long period of ≈47 days. To place this point in perspective, MARVELS-6b is plotted against a catalog of BDs from Ma & Ge (2013) in Figure 14. Two aspects of this plot are particularly interesting. First, MARVELS-6b is in an underdense region in period space. In the inset of Figure 14, there is a clear rise in the envelope of eccentricity as one moves to larger periods until one reaches roughly 200 days. MARVELS-6b is either on or below the bottom edge of this envelope. There is the possibility that this effect is due to observational bias; for low S/N, one often measures a non-zero eccentricity even when the true eccentricity is zero. For a given radial velocity precision and companion mass, longer periods will have lower S/N (since the semi-amplitude is smaller), and so the lack of low eccentricity companions at long periods could be due to this effect. In any case, there are so few BD in this plot that it is not clear whether MARVELS-6b's low eccentricity is significant, so further comment on this will have to wait until more data is available.

This BD companion is also an outlier in metallicity space. In Figure 15, MARVELS-6b is again plotted with the BD from Ma & Ge (2013). GSC 03546-01452's metallicity is significantly super solar and MARVELS-6b exists in an empty region of eccentricity-metallicity space. As in the previous figure, the plot is merely suggestive of interesting astrophysics, but there are not a sufficient number of BDs to know whether MARVELS-6b is a significant deviation. MARVELS-6b is helping to fill in the BD parameter space, and with more data its location may become more astrophysically significant.

5. CONCLUSION

In this paper, we report the discovery of a BD companion to GSC 03546-01452 with a minimum mass of 31.7 ± 2.0 $M_{\rm Jup}$. This BD, designated MARVELS-6b, has a moderately long period of $47.8929^{+0.0063}_{-0.0062}$ days with a low eccentricity of $0.1442^{+0.0078}_{-0.0073}$. We have analyzed moderate resolution spectroscopy of the host star and have determined the following properties: $T_{\rm eff} = 5598 \pm 63$, $\log g = 4.44 \pm 0.17$, and [Fe/H] = +0.40 ± 0.09. From these measurements we find that GSC 03546-01452 has a mass and radius of $M_* = 1.11 \pm 0.11\,M_\odot$ and $R_* = 1.06 \pm 0.23\,R_\odot$. This result combined with photometry, indicates the host star is a G dwarf at 219 ± 21 pc from the Sun with an age less than approximately 6 Gyr based on an evolutionary track analysis.

Due to its moderately long period, MARVELS-6b has a transit probability for a uniform distribution of $\cos i$ of only 1.8%. Although we have roughly 13,000 photometric data points, we cannot conclusively rule out a transit. In the Keck AO imaging, no visual companions were found. However, in the LI, a previously known companion at 7.″7 from the host star was detected. This visual companion appears in both the 2MASS and KIC catalogs, and was shown not be a physical companion based upon photometry and astrometry, which is unexpected given that many of the previous BD found by the MARVELS survey did have tertiary companions.

Finally, we found that minimum mass of MARVELS-6b exists at the minimum of the mass functions of close (orbital period <5 yr) stellar and planetary companions to stars, making this a rare object even compared to other BDs. It also exists in an underdense region in both period/eccentricity and metallicity/eccentricity space. This ultimately furthers the goal of this series of papers, to help fill out the low-mass companion phase space, which will ultimately help us understand these intriguing objects.

The SuperWASP and Allegheny lightcurve data for GSC 03546-01452 , along with the APO spectroscopic data, will be made available through the Vizier/CDS[28] catalog service. The SuperWASP and Allegheny lightcurve data will also be available with the online edition of this article.

[28] http://vizier.u-strasbg.fr/viz-bin/VizieR

Funding for the MARVELS multi-object Doppler instrument was provided by the W. M. Keck Foundation and NSF with grant AST-0705139. The MARVELS survey was partially funded by the SDSS-III consortium, NSF grant AST-0705139, NASA with grant NNX07AP14G and the University of Florida.

Funding for SDSS-III has been provided by the Alfred P. Sloan Foundation, the Participating Institutions, the National Science Foundation, and the U.S. Department of Energy Office of Science. The SDSS-III Web site is http://www.sdss3.org/.

SDSS-III is managed by the Astrophysical Research Consortium for the Participating Institutions of the SDSS-III Collaboration including the University of Arizona, the Brazilian Participation Group, Brookhaven National Laboratory, University of Cambridge, Carnegie Mellon University, University of Florida, the French Participation Group, the German Participation Group, Harvard University, the Instituto de Astrofisica de Canarias, the Michigan State/Notre Dame/JINA Participation Group, Johns Hopkins University, Lawrence Berkeley National Laboratory, Max Planck Institute for Astrophysics, Max Planck Institute for Extraterrestrial Physics, New Mexico State University, New York University, Ohio State University, Pennsylvania State University, University of Portsmouth, Princeton University, the Spanish Participation Group, University of Tokyo, University of Utah, Vanderbilt University, University of Virginia, University of Washington, and Yale University.

Based on observations made with the Italian Telescopio Nazionale Galileo (TNG) operated on the island of La Palma by the Fundación Galileo Galilei of the INAF (Istituto Nazionale di Astrofisica) at the Spanish Observatoriodel Roque de los Muchachos of the Instituto de Astrofisica de Canarias. The Center for Exoplanets and Habitable Worlds is supported by the Pennsylvania State University, the Eberly College of Science, and the Pennsylvania Space Grant Consortium. Keivan Stassun, Leslie Hebb, and Joshua Pepper acknowledge funding support from the Vanderbilt Initiative in Data-Intensive Astrophysics (VIDA) from Vanderbilt University, and from NSF Career award AST-0349075. B.S.G. and J.D.E. acknowledge support from NSF CAREER grant AST-1056524. E.A. thanks NSF for CAREER grant 0645416. G.F.P.M. acknowledges financial support from CNPq grant No. 476909/2006-6 and FAPERJ grant No. APQ1/26/170.687/2004. L.G. acknowledges financial support provided by the PAPDRJ CAPES/FAPERJ Fellowship.

Facility: Sloan

REFERENCES

Baluev, R. V. 2008, MNRAS, 385, 1279
Baraffe, I., Chabrier, G., Barman, T. S., Allard, F., & Hauschildt, P. H. 2003, A&A, 402, 701
Bensby, T., Feltzing, S., & Lundström, I. 2003, A&A, 410, 527
Borucki, W. J., Koch, D., Basri, G., et al. 2010, Sci, 327, 977
Brown, T. M., Latham, D. W., Everett, M. E., & Esquerdo, G. A. 2011, AJ, 142, 112
Burke, C. J., Gaudi, B. S., DePoy, D. L., & Pogge, R. W. 2006, AJ, 132, 210
Chabrier, G., Baraffe, I., Allard, F., & Hauschildt, P. 2000, ApJ, 542, 464
Claret, A., & Hauschildt, P. H. 2003, A&A, 412, 241
Collier Cameron, A., Wilson, D. M., West, R. G., et al. 2007, MNRAS, 380, 1230
Coşkunoğlu, B., Ak, S., Bilir, S., et al. 2011, MNRAS, 412, 1237
Cumming, A. 2004, MNRAS, 354, 1165
Cutri, R. M., Skrutskie, M. F., van Dyk, S., et al. 2003, 2MASS All-Sky Catalog
Delfosse, X., Forveille, T., Ségransan, D., et al. 2000, A&A, 364, 217
Demarque, P., Woo, J., Kim, Y., & Yi, S. K. 2004, ApJS, 155, 667
Duquennoy, A., & Mayor, M. 1991, A&A, 248, 485
Eastman, J., Gaudi, B. S., & Agol, E. 2013, PASP, 125, 83
Eisenstein, D. J., Weinberg, D. H., Agol, E., et al. 2011, AJ, 142, 72
Erskine, D. J. 2003, PASP, 115, 255
Femenía, B., Rebolo, R., Pérez-Prieto, J. A., et al. 2011, MNRAS, 413, 1524
Fleming, S. W., Ge, J., Barnes, R., et al. 2012, AJ, 144, 72
Fleming, S. W., Ge, J., Mahadevan, S., et al. 2010, ApJ, 718, 1186
Ford, E. B. 2006, ApJ, 642, 505
Fukugita, M., Ichikawa, T., Gunn, J. E., et al. 1996, AJ, 111, 1748
Ge, J. 2002, ApJL, 571, L165
Ge, J., & Eisenstein, D. 2009, astro2010: The Astronomy and Astrophysics Decadal Survey, 86
Ge, J., Erskine, D. J., & Rushford, M. 2002, PASP, 114, 1016
Ge, J., Lee, B., de Lee, N., et al. 2009, Proc. SPIE, 7440, 74400L
Ge, J., Mahadevan, S., Lee, B., et al. 2008, in ASP Conf. Ser. 398, Extreme Solar Systems, ed. D. Fischer, F. A. Rasio, S. E. Thorsett, & A. Wolszczan (San Francisco, CA: ASP), 449
Ge, J., van Eyken, J., Mahadevan, S., et al. 2006, ApJ, 648, 683
Gratton, R. G., Bonanno, G., Bruno, P., et al. 2001, ExA, 12, 107
Grether, D., & Lineweaver, C. H. 2006, ApJ, 640, 1051
Griffin, R., & Griffin, R. 1973, MNRAS, 162, 255
Gunn, J. E., Siegmund, W. A., Mannery, E. J., et al. 2006, AJ, 131, 2332
Haghighipour, N., Vogt, S. S., Butler, R. P., et al. 2010, ApJ, 715, 271
Halbwachs, J. L., Mayor, M., Udry, S., & Arenou, F. 2003, A&A, 397, 159
Hauschildt, P. H., Allard, F., & Baron, E. 1999, ApJ, 512, 377
Henry, T. J. 2004, in ASP Conf. Ser. 318, Spectroscopically and Spatially Resolving the Components of the Close Binary Stars, ed. R. W. Hilditch, H. Hensberge, & K. Pavlovski (San Francisco, CA: ASP), 159
Henry, T. J., Franz, O. G., Wasserman, L. H., et al. 1999, ApJ, 512, 864
Howard, A. W., Johnson, J. A., Marcy, G. W., et al. 2010, ApJ, 721, 1467
Jiang, P., Ge, J., Cargile, P., et al. 2013, AJ, submitted
Johnson, D. R. H., & Soderblom, D. R. 1987, AJ, 93, 864
Landolt, A. U. 2009, AJ, 137, 4186
Landolt, A. U., & Uomoto, A. K. 2007, AJ, 133, 768
Lasker, B. M., Lattanzi, M. G., McLean, B. J., et al. 2008, AJ, 136, 735
Lee, B. L., Ge, J., Fleming, S. W., et al. 2011, ApJ, 728, 32
Lomb, N. R. 1976, Ap&SS, 39, 447
Ma, B., & Ge, J. 2013, arXiv:1303.6442
Ma, B., Ge, J., Barnes, R., et al. 2013, AJ, 145, 20
Mack, C. E., III, Ge, J., Deshpande, R., et al. 2013, AJ, 145, 139
Mamajek, E. 2010, A Modern Dwarf Stellar Effective Temperature Scale Based on 17842 Teff and MK Spectral Type Pairs, http://www.pas.rochester.edu/emamajek/Teff_SpT_table.txt
Mandel, K., & Agol, E. 2002, ApJL, 580, L171
Marcy, G. W., & Butler, R. P. 2000, PASP, 112, 137
Marcy, G. W., & Butler, R. P. 1992, PASP, 104, 270
Markwardt, C. B. 2009, in ASP Conf. Ser. 411, Astronomical Data Analysis Software and Systems XVIII, ed. D. A. Bohlender, D. Durand, & P. Dowler (San Francisco, CA: ASP), 251
Mayor, M., Pepe, F., Queloz, D., et al. 2003, Msngr, 114, 20
Morrissey, P., Conrow, T., Barlow, T. A., et al. 2007, ApJS, 173, 682
Oscoz, A., Floyd, D., & Covarrubias, R. 2008, Proc. SPIE, 7014, 701447
Patel, S. G., Vogt, S. S., Marcy, G. W., et al. 2007, ApJ, 665, 744
Pollacco, D. L., Skillen, I., Collier Cameron, A., et al. 2006, PASP, 118, 1407
Reid, I. N., & Metchev, S. A. 2008, in Exoplanets: Detection, Formation, Properties, Habitability, ed. J. W. Mason (Berlin: Springer), 115
Sahlmann, J., Ségransan, D., Queloz, D., et al. 2011, A&A, 525, A95
Scargle, J. D. 1982, ApJ, 263, 835
Schlegel, D. J., Finkbeiner, D. P., & Davis, M. 1998, ApJ, 500, 525
Skrutskie, M. F., Cutri, R. M., Stiening, R., et al. 2006, AJ, 131, 1163
Smith, J. A., Tucker, D. L., Kent, S., et al. 2002, AJ, 123, 2121
Sneden, C. 1973, PhD thesis, Univ. of Texas-Austin
Spiegel, D. S., Burrows, A., & Milsom, J. A. 2011, ApJ, 727, 57
Torres, G., Andersen, J., & Giménez, A. 2010, A&ARv, 18, 67
Udry, S., Mayor, M., Naef, D., et al. 2000, A&A, 356, 590
Udry, S., & Santos, N. C. 2007, ARA&A, 45, 397
van Eyken, J. C., Ge, J., & Mahadevan, S. 2010, ApJS, 189, 156
Wang, J., Ge, J., Jiang, P., & Zhao, B. 2011, ApJ, 738, 132
Wang, J., Ge, J., Wan, X., De Lee, N., & Lee, B. 2012a, PASP, 124, 1159
Wang, J., Ge, J., Wan, X., Lee, B., & De Lee, N. 2012b, PASP, 124, 598
Wang, S., Hildebrand, R. H., Hobbs, L. M., et al. 2003, Proc. SPIE, 4841, 1145
Wisniewski, J. P., Ge, J., Crepp, J. R., et al. 2012, AJ, 143, 107
Wizinowich, P., Acton, D. S., Shelton, C., et al. 2000, PASP, 112, 315
Wright, E. L., Eisenhardt, P. R. M., Mainzer, A. K., et al. 2010, AJ, 140, 1868
Xia, F., & Fu, Y.-N. 2010, ChA&A, 34, 277
Xia, F., Ren, S., & Fu, Y. 2008, Ap&SS, 314, 51
Zacharias, N., Finch, C. T., Girard, T. M., et al. 2013, AJ, 145, 44